Biochemical and Biophysical Research Communications 437 (2013) 29–34

Contents lists available at SciVerse ScienceDirect

Biochemical and Biophysical Research Communications

journal homepage: www.elsevier.com/locate/ybbrc

Mitochondrial function is impaired in yeast and human cellular models of Shwachman Diamond syndrome

Adrianna L. Henson [a], Joseph B. Moore IV [a], Pascale Alard [b], Max M. Wattenberg [a], Johnson M. Liu [c], Steven R. Ellis [a,*]

[a] Department of Biochemistry and Molecular Biology, University of Louisville, United States
[b] Department of Microbiology and Immunology, University of Louisville, United States
[c] The Feinstein Institute of Medical Research, Manhasset, NY, United States

ARTICLE INFO

Article history:
Received 6 June 2013
Available online 19 June 2013

Keywords:
Bone marrow failure
Mitochondria
Ribosome
Translation

ABSTRACT

Shwachman Diamond syndrome (SDS) is an inherited bone marrow failure syndrome typically characterized by neutropenia, exocrine pancreas dysfunction, metaphyseal chondrodysplasia, and predisposition to myelodysplastic syndrome and leukemia. *SBDS*, the gene affected in most cases of SDS, encodes a protein known to influence many cellular processes including ribosome biogenesis, mitotic spindle assembly, chemotaxis, and the regulation of reactive oxygen species production. The best characterized role for the SBDS protein is in the production of functional 60S ribosomal subunits. Given that a reduction in functional 60S subunits could impact on the translational output of cells depleted of SBDS we analyzed protein synthesis in yeast cells lacking *SDO1*, the ortholog of *SBDS*. Cells lacking *SDO1* selectively increased the synthesis of *POR1*, the ortholog of mammalian *VDAC1* a major anion channel of the mitochondrial outer membrane. Further studies revealed the cells lacking *SDO1* were compromised in growth on non-fermentable carbon sources suggesting mitochondrial function was impaired. These observations prompted us to examine mitochondrial function in human cells where *SBDS* expression was reduced. Our studies indicate that reduced expression of SBDS decreases mitochondrial membrane potential and oxygen consumption and increases the production of reactive oxygen species. These studies indicate that mitochondrial function is also perturbed in cells expressing reduced amounts of SBDS and indicate that disruption of mitochondrial function may also contribute to SDS pathophysiology.

1. Introduction

Shwachman Diamond syndrome (SDS, OMIM #260400) is a rare bone marrow failure syndrome characterized by neutropenia, exocrine pancreas insufficiency, metaphyseal chondrodysplasia, and predisposition to myelodysplastic syndrome and leukemia [1]. The gene affected in most cases of SDS is *SBDS*, which encodes a highly conserved protein found in eukaryotes and archaebacteria [2]. Studies in yeast and mammalian cells have shown that members of the SBDS family of proteins are required for the biogenesis of the 60S ribosomal subunit via a role for SBDS in releasing eIF-6 from maturing subunits in the cytoplasm [3–6]. The continued association of eIF-6 with 60S subunits prevents their association with 40S subunits in forming active 80S ribosomes and the inability to recycle eIF-6 back to the nucleolus eventually interferes with the role of this factor in transporting pre-60S subunits from the nucleus to the cytoplasm. Thus, cells depleted of SBDS family members exhibit a deficiency of active 60S subunits and subsequent effects on translation are evidenced by the appearance of half-mer polysomes.

In addition to its role in ribosome synthesis, SBDS has been implicated in other cellular processes including mitotic spindle assembly, chemotaxis, and in the regulation of reactive oxygen species generation; suggesting that SBDS may be a multifunctional protein [7–9]. Given the potential pleiotropic effects of disruptions in ribosome synthesis mediated by downstream effects on protein synthesis, it is possible that some of these additional functions attributed to SBDS may be a consequence of indirect effects on translational output.

To examine the effects of depletion of SBDS family members on translational output, we turned to the yeast model of SDS using cells lacking Sdo1, the yeast ortholog of SBDS. Yeast cells lacking Sdo1 exhibit a very slow growth phenotype on fermentable carbon sources, with dramatic effects on the translational machinery as evidenced by pronounced half-mer polysomes [4]. To address effects specific to Sdo1 depletion, as opposed to general effects on translation resulting from a 60S subunit deficit, we compared the translational output of cells depleted of Sdo1 with that of cells

* Corresponding author. Address: Department of Biochemistry and Molecular Biology, University of Louisville, Louisville, KY 40292, United States.
E-mail address: srellis@louisville.edu (S.R. Ellis).

0006-291X/$ - see front matter © 2013 Elsevier Inc. All rights reserved.
http://dx.doi.org/10.1016/j.bbrc.2013.06.028

depleted of ribosomal protein Rpl33a (representing a yeast model of Diamond Blackfan anemia). Our analysis revealed that Por1, an ortholog of the mammalian VDAC1, is specifically induced in cells depleted of Sdo1.

VDAC1 encodes a mitochondrial voltage dependent anion channel which has been reported to be a component of the mitochondrial permeability pore in mammalian cells [10]. Both increased and reduced expression of VDAC1 in cells has been shown to disrupt mitochondrial function and induce apoptosis. Consequently, we investigated the effects of depleting cells of Sdo1 on respiratory growth. Our data reveal that depletion of Sdo1 affects respiratory growth in yeast and that mitochondrial function is also disrupted in human hematopoietic cells depleted of SBDS.

2. Materials and methods

2.1. Yeast strains

The yeast strains used in this study were initially generated by the *Saccharomyces* genome deletion project and were either obtained from Research Genetics or Euroscarf. The heterozygous diploid for *SDO1* was (20519D: MAT a/α *ura3-1/ura3-1*, *his3-11/his3-11*, *leu2-3_112/leu2-3_112*, *trp1Δ2/trp1Δ2*, *ade2-1/ade2-1*, *can1-100/can1-100*, *sdo1::kanMX4/SDO1*). A heterozygous diploid for *RPL33A* in the same W303 genetic background as that for *SDO1* was created as described previously [4]. The genotype of the *RPL33A* strain used here was MAT a/α *ura3-1/ura3-1*, *his3-11/his3-11*, *leu2-3_112/leu2-3_112*, *trp1Δ2/trp1Δ2*, *ade2-1/ade2-1*, *can1-100/can1-100*, *rpl33A::kanMX4/RPL33A*. Because of a high spontaneous suppression rate of both *SDO1* and *RPL33A* mutants, haploid strains were freshly derived for each experiment.

2.2. Human cell lines, culture conditions, and cytokines

Human TF-1 erythroleukemic cell lines transduced with lentiviral vectors targeting SBDS mRNA using one of two sequences (#1 or #2) were established as previously described (Sezgen et al., Ped. Blood Cancer, in press). Clones were used if they expressed less than 35% of control levels of SBDS mRNA by qRT-PCR. TF-1 cell lines were cultured in RPMI media (Mediatech) supplemented with 10% FBS (Mediatech), 1% pen-strep (Invitrogen) and 5 ng/mL GM-CSF (Preprotech).

2.3. Pulse labeling of yeast and two-dimensional gel electrophoretic separation of newly synthesized proteins

Synthetic complete glucose media lacking methionine (SC-Met, 40 ml) was inoculated with the different yeast strains and allowed to grow to an optical density (600 nm) of 0.2. Cells were collected by centrifugation and resuspended in 1 ml of SC-Met media and incubated with 100 μCi of [^{35}S]-methionine for 30 min. Total protein was then isolated from samples using a variation in the method outlined by Futcher et al. [11]. Following protein isolation, 50 μg of total protein was prepared and isoelectric focusing performed using pH 3–10 Broad Range ZOOM® Strips in conjunction with the ZOOM® IPGRunner System (Invitrogen) as directed by the manufacturer. Subsequently, IEF strips were prepared and the second dimension resolved by SDS–PAGE gel analysis, as instructed by the manufacture, using NuPAGE® Novex 4–12% Bis–Tris ZOOM® gels (Invitrogen).

2.4. Western blotting

Cells were pelleted by centrifugation, and lysed in RIPA buffer containing leupeptin, aprotinin, PMSF, and protease inhibitor cocktail (Sigma). Equal amounts of total protein were suspended in Nupage buffer (Invitrogen) and DTT (Sigma) and proteins separated on 4–12% Bis–Tris gels (Invitrogen). Proteins were transferred to nitrocellulose membranes (Biorad), blocked with 5% milk in TBST (Fisher) and immunoblotted with antibodies to either: anti-SBDS (SC-39257, Santa Cruz; 1:1000), anti-eIF6 (10291-1-AP, Proteintech; 1:1500), anti-VDAC1 (4661, Cell Signaling; 1:1000), and anti-β-Actin (SC69879 AC-15 Santa Cruz; 1:5000). HRP-linked secondary antibodies included: goat anti-mouse (#3430 Thermo Scientific and Santa Cruz), and goat anti-rabbit (7074, Cells Signaling). Antibody complexes were detected with enhanced chemiluminescent reagent (GE) after exposure to film from Denville Scientific. Signal intensity was quantified using Image software (NIH).

2.5. Oxygen consumption

Oxygen consumption by TF-1 cell lines was measured using a Gilson oxygraph with a Clark-type electrode following published protocols [12,13]. The instrument was calibrated using growth media for the maximal concentration of oxygen and media depleted of oxygen using sodium bisulfite to establish baseline. Cells were suspended in 550 μL of growth media at a concentration of 2.7×10^6 cells/ml and placed in the chamber. Basal respiration tracings of oxygen consumption were read for two minutes. Carbonyl cyanide *m*-chlorophenyl hydrazine (CCCP, Sigma) was added to the chamber using a Hamilton Syringe to a final concentration of 1 mM to measure maximal respiration over 8 min period. Respiration rates were expressed as μmol of oxygen consumed per million cells per minute. Linear portions of the curve were used to express respiration as a ratio of basal respiration relative to maximal respiration. Data shown are averages of three independent experiments.

2.6. Mitochondrial membrane potential measurements

Mitochondrial membrane potential of TF-1 cell lines was assessed using JC-1 assay kit from Molecular Probes according to the manufacturer's instructions. Pretreatment with 50 mM CCCP served as a negative control and unstained cells served as a control for autofluorescence. After incubation with the JC-1 compound for 20 min at 37 °C the cells were harvested and suspended in PBS for analysis with the BD FACS Calibur cytometer (BD Biosciences). Plots of side and forward scatter were used to determine the total number of live cells. The FL2 channel was used to measure red fluorescence and was graphically represented on the *y*-axis and the FL-1 channel used to measure green fluorescence was graphed on the *x*-axis. The upper right quadrant represents cells with high green and red fluorescence whereas the lower right quadrant represents cells with increased ratio of green to red fluorescence indicative of a decrease in membrane potential. A minimum of 40,000 events were collected for each sample replicate, and data shown are representative of three independent experiments. Analysis was performed using FlowJo software from Treestar to perform appropriate compensation, gating, and comparison of all replicate data.

2.7. Reactive oxygen species generation

Reactive oxygen species were detected in TF-1 cell lines with 2′,7′-dichlorofluorescein-diacetate (DCFHDA) [9]. Cells were plated at a density of 1×10^5 cells/well. DCFHDA (Sigma) in DMSO was added to a final concentration of 20 μM. After incubation at 37 °C for 15 min, the plates were then read every minute using wavelengths of 505 nm for excitation and 529 nm for emission using an Agilent Bioanalyzer. After subtracting for fluorescence with vehicle alone values were presented as a ratio of SBDS knockdowns

relative to scrambled controls. A minimum of three replicates were performed in each experiment.

2.8. Statistical analysis

All data represent a minimum of three independent experiments. Microsoft's Excel program and Graphpad's Prism software were used to perform all statistical analyses of the data. When appropriate, an unpaired Student's *t*-test was used to determine the significance of differences between sample means. When more than two sample categories were analyzed, such as VDAC expression with different lentiviral vectors targeting SBDS, a one-way ANOVA was used followed by the appropriate post-test using Graphpad Prism.

3. Results

Although previous data demonstrated a role for SBDS family members in ribosome biogenesis, it is unclear whether defects in ribosome synthesis *per se* are responsible for phenotypes linked to reduced expression or whether phenotypes might be linked to downstream effects on protein synthesis. To address potential effects of loss of Sdo1 on yeast protein synthesis, cells were pulse labeled with [^{35}S]-Met for 30 min and newly synthesized proteins were analyzed by two-dimensional gel electrophoresis. Fig. 1 shows the results for the Δ*SDO1* strain compared with an isogenic wild-type control. One of the more obvious differences between the two strains is shown in the insets where the patterns of proteins synthesized could be readily overlaid. The three bands in the center that appear to shift in relative amounts between the mutant and wild-type are different forms of glyceraldehyde 3-phosphate dehydrogenase (data not shown). While potentially interesting, this difference was not pursued further. Instead we chose to focus on the signal in the lower right of the mutant inset, which is dramatically increased in the mutant relative to wild-type. Proteins were recovered from this spot and subjected to MALDI-TOF sequence analysis. The results indicated that this signal was from Por1, the yeast ortholog of the human voltage dependent anion channel (VDAC1).

To confirm increased expression of Por1 protein in mutant versus wild-type cells, extracts from the two cell strains were immunoblotted with antisera to Por1. Supplemental Fig. 1A top panel shows that the steady-state levels of the Por1 protein are indeed dramatically increased relative to the actin control in cells lacking Sdo1 compared with control. Extracts from a strain where the *RPL33A* was deleted was also included in this analysis to control for a general reduction in 60S subunits [4]. The protein data summarized in Supplemental Fig. 1B reveal that the steady-state levels of Por1 are increased approximately 4-fold in the Δ*SDO1* strain relative to wild-type and the *RPL33A* mutant, indicating that the increase is selective for the Δ*SDO1* strain. Analysis of the steady-state levels of the mRNAs for Por1 when normalized to actin indicates very little change in mRNA levels between the 3 strains (Supplemental Fig. 1C). Thus, the increase in Por1 levels appears to be a consequence of post-transcriptional mechanisms.

Por1 is a mitochondrial porin in yeast required for growth on non-fermentable carbon sources at elevated temperatures [14]. We are unaware of any data addressing the consequences of overexpression of Por1 on mitochondrial function in yeast. We did however have evidence suggesting that mitochondrial function might be disrupted in yeast cells lacking Sdo1. Analysis of the colony color in tetrads arising from dissection of a diploid strain heterozygous for the *SDO1* deletion revealed that the small colonies arising from deleted spores lacked the red color associated with the outgrowth of wild-type spores (Supplemental Fig. 2, panel A). The red color results from the accumulation of a pigmented intermediate in the adenine synthesis pathway in strains with the *ade2-1* allele. A source of electrons is required for robust color development, and strains unable to respire lack the intensely colored red pigment [15]. The color differences were not simply a consequence of the difference in growth rate between the *SDO1* mutant and wild-type as the slow growing *RPL33A* mutants develop red color (Supplemental Fig. 2, panel B). Panel C shows that both the growth defect and red colony color in the Δ*SDO1* cells are rescued by plasmid-borne *SDO1*. These data therefore suggested that the Δ*SDO1* strain has impaired respiratory function.

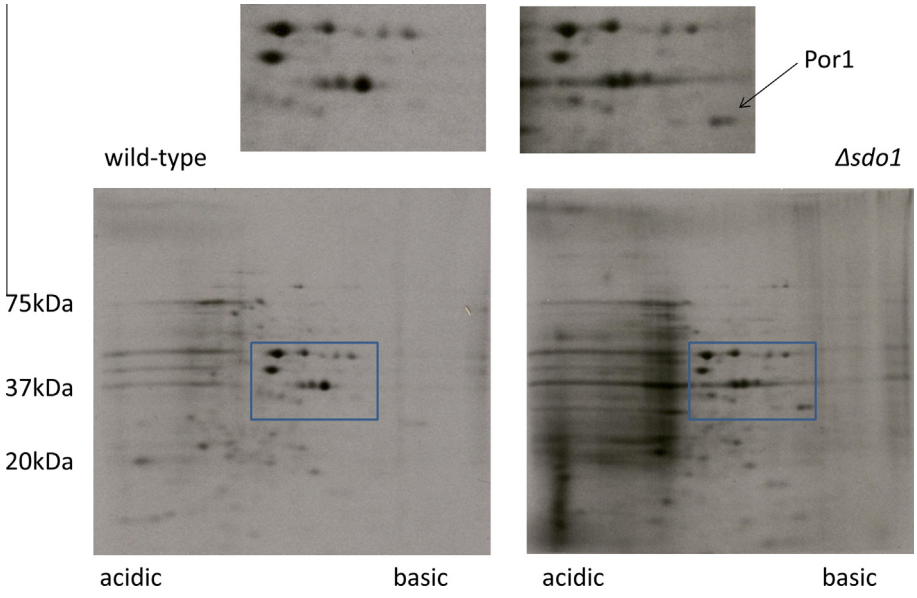

Fig. 1. Proteomic analysis of the Δ*SDO1* strain relative to control cultures. Wild-type (left panels) and Δ*SDO1* (right panels) strains were incubated for 30 min with [^{35}S]-methionine. Total protein extracts were resolved by 2D gel electrophoresis. The pH gradient for IEF was 3–10. The second dimension was resolved via a 4–12% polyacrylamide gel. Molecular masses for size standards are shown to the left. Regions enclosed by the boxes are expanded above each gel. The spot labeled Por1 in the inset was excised and identified via MALDI-TOF mass spectrometry.

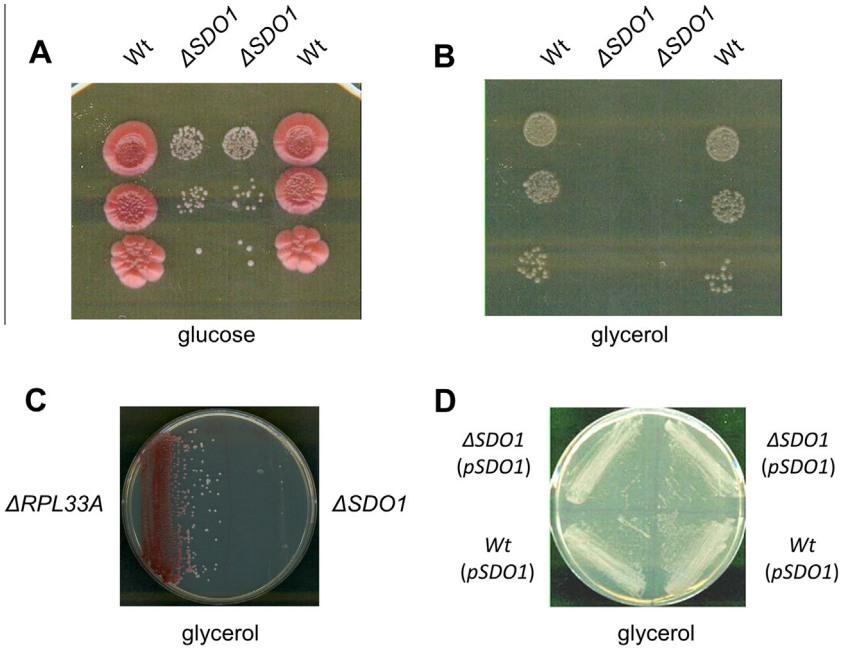

Fig. 2. Growth defects of ΔSDO1 cells on non-fermentable carbon sources. Top panel: Serial dilutions of Wt and ΔSDO1 strains on glucose (A) or glycerol (B)-containing media. Cells were grown for 3–5 days at 30°. Panel C compares the growth of individual cultures of ΔSDO1 and RPL33a on glycerol-containing media. Panel D, rescue of the respiratory-deficient phenotype of ΔSDO1 cells by plasmid-borne *SDO1*.

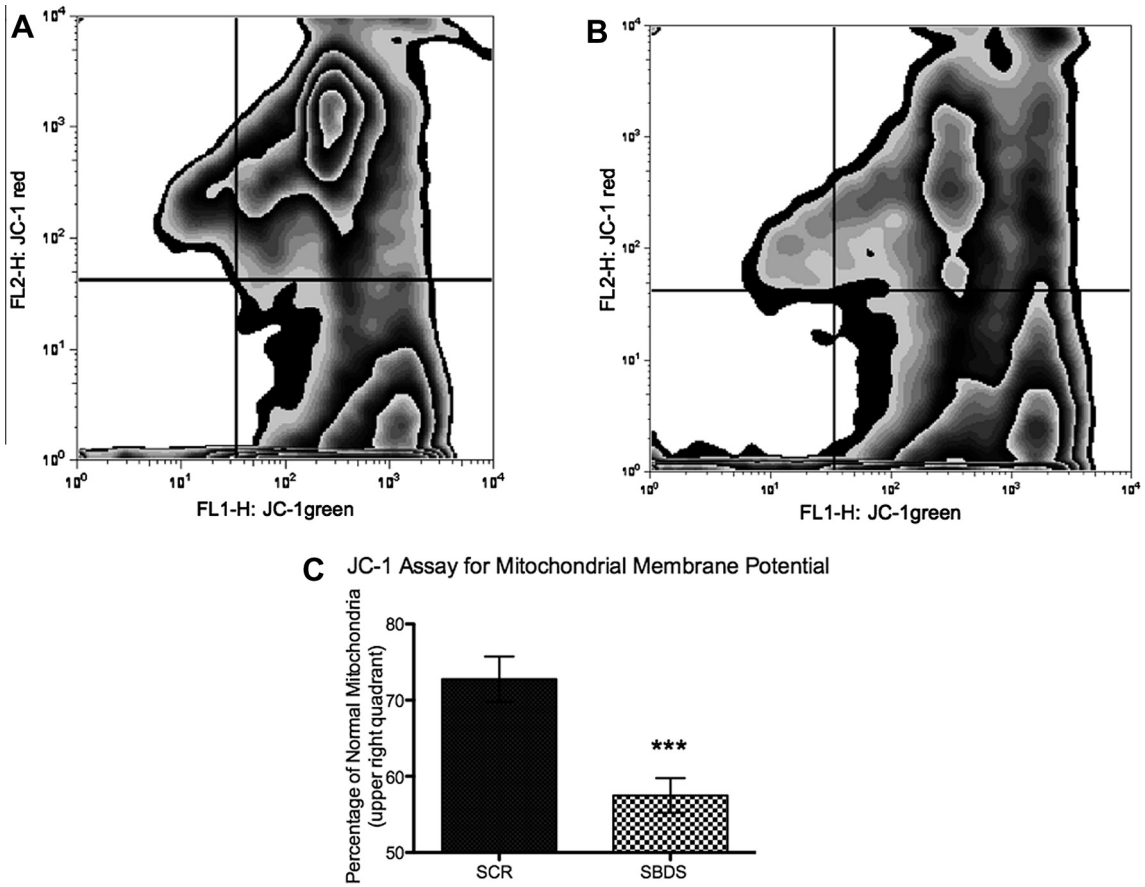

Fig. 3. Mitochondrial membrane potential is decreased in TF-1 cells expressing reduced amounts of SBDS. Top panel: representative plots of TF-1 cells transduced with Scr control (A) or SBDS (B) vectors. Cells were treated with JC-1 which undergoes a fluorescence emission spectrum shift from green to red when it is retained within the mitochondria forming red "J-aggregates." Cells were subjected to FACS analysis. Bottom panel: Replicate data from three independent experiments comparing the percentage of cells in the upper right quadrant defined as normal mitochondrial membrane potential for TF-1 cells. Error bars represent S.E.M. ($n = 3$, $^{***}p < 0.001$).

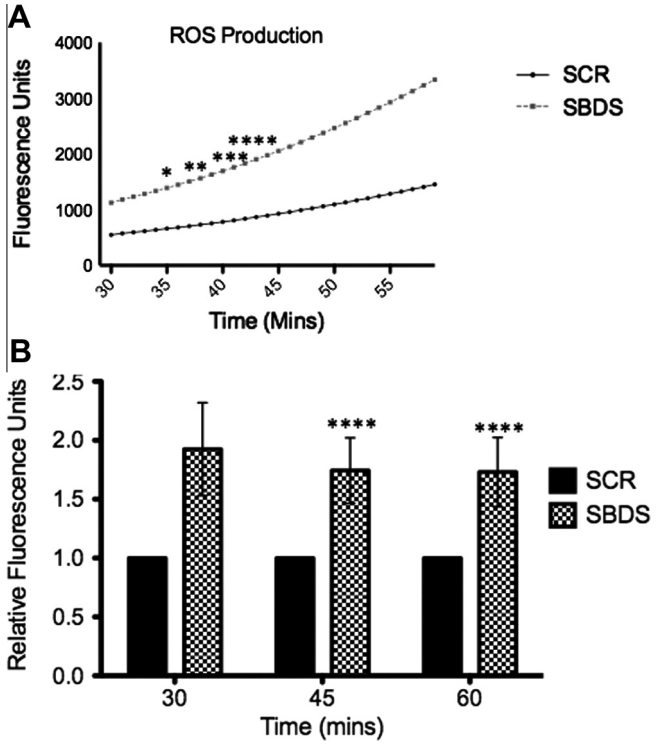

Fig. 4. Increased ROS production with SBDS knockdown. DCFHDA was added to TF-1 cells depleted of SBDS or control samples and generation of a fluorescent product measured every minute for 1 h. (A) Representative fluorescence emission with time after treatment with DCFHDA. (B) Average fold increase in ROS production in SBDS depleted samples relative to scrambled control. Error bars represent S.D. ($^{*}p < 0.05$ $^{**}p < 0.01$ $^{***}p < 0.001$ $^{****}p < 0.0001$).

To address respiratory capacity of the Δ*SDO1* strain, we examined growth on plates containing the non-fermentable carbon source glycerol. Colonies arising from spores within a tetrad from a Δ*SDO1* heterozygous diploid were dispersed in water, normalized for light scattering at 600 nm, and spotted with serial dilutions on rich media containing fermentable (glucose) or non-fermentable (glycerol) carbons sources. The results from this analysis reveal complex phenotypes associated with the *SDO1* deletion. First, as evident from the spots on fermentable media, the number of colonies arising in the mutant samples compared to wild-type is reduced (Fig. 2, panel A). This reduction is a reflection of reduced viability of the mutant cells evident by microscopic examination where many of the cells spotted fail to divide. On glycerol, the vast majority of cells fail to divide and give rise to observable colonies with the exception of an extremely small number of micro colonies that begin to develop within the most concentrated spots over time (Fig. 2, panel B/C). We believe that these colonies arise from some type of suppression event that allows respiratory growth without substantially affecting growth rate on fermentable carbon sources. While the nature of this suppression event is unknown at the present time, sequencing of the *TIF6* gene from these colonies indicates that it does not involve missense mutations in this gene, which have been shown to suppress generalized growth defects of Δ*SDO1* cells [3] (data not shown). As shown in Fig. 2, panel D the plasmid-borne *SDO1* can rescue glycerol growth of Δ*SDO1* cells.

The results in yeast indicate that mitochondrial function is disrupted in cells lacking Sdo1. We therefore asked whether there were effects on mitochondrial function in human cells depleted of SBDS. The cells used for these studies were the human erythroleukemia cell line, TF1. Expression of SBDS was reduced after transduction with a lentivirus vector expressing one of two shRNA sequences targeting SBDS mRNA as described previously [16]. A scrambled control cell line was also created by transducing cells with a lentiviral non-targeting sequence. The expression of the SBDS protein was decreased to nearly undetectable levels based on Western blotting (Supplemental Fig. 3). Like yeast samples depleted of Sdo1, these samples had a statistically significant and reproducible increase in protein expression of VDAC1 (Supplemental Fig. 3).

Mitochondrial function in TF-1 cells depleted of SBDS was assessed by measuring mitochondrial membrane potential and oxygen consumption. The mitochondrial membrane potential of these cells was examined using 5,5′,6,6′-tetrachloro-1,1′,3,3′-tetraethylbenzimi-dazolylcarbocyanine iodide (JC-1), a lipophilic cationic dye and subsequent FACS analysis of fluorescence emission. In this assay, the ratio of red to green fluorescence is an indicator of mitochondrial membrane potential. Fig. 3 shows that the ratio of red to green fluorescence is dramatically decreased in cells expressing reduced amounts of SBDS relative to scrambled controls. Similarly, cells expressing reduced amounts of SBDS exhibit decreased oxygen consumption relative to control cells (Supplemental Fig. 4). These data indicate that mitochondrial function is also compromised in human cells depleted of SBDS.

Previous studies in cellular models of SDS have indicated an increase in reactive oxygen species (ROS) in cells expressing reduced amounts of SBDS [1]. As mitochondria are major sources of ROS in cells and increases in ROS generation frequently accompany defects in mitochondrial function [13,17], we examined ROS levels in the TF1 cells used here that were depleted of SBDS. Fig. 4 shows that ROS levels are increased in TF1 cells depleted of SBDS relative to scrambled controls.

4. Discussion

The results presented here indicate that mitochondrial function is disrupted in yeast and human cell models of SDS. Our interest in mitochondrial function in these models arose from our observation that the expression of the mitochondrial porin, Por1, is dramatically increased in yeast cells lacking Sdo1. Por1 is the yeast ortholog of VDAC1, a mitochondrial voltage dependent anion channel. VDAC1 has been reported to be a component of the mitochondrial permeability pore and plays an important (but still controversial) role in apoptosis in mammalian cells. Both over and under-expression of VDAC1 in mammalian systems has been associated with impaired mitochondrial function and enhanced apoptosis [18–26].

When tested for growth on the non-fermentable carbon source glycerol, Δ*RPL33A* cells were capable of growth whereas Δ*SDO1* were not. Thus, although both of these strains have a deficiency of functional 60S subunits in the cytoplasm as evidenced by the presence of half-mer polysomes [4], the mechanisms underlying these deficiencies have profoundly different effects on growth on respiratory carbon sources. The mechanism underlying the 60S subunit deficiency in Δ*RPL33A* cells is abortive subunit assembly linked to suboptimal amounts of Rpl33A. In contrast, loss of Sdo1 influences the release of the anti-association factor Tif6 from 60S subunits in the cytoplasm which in turn influences Tif6 recycling back to the nucleus where it participates in the transport of pre-60S subunits from the nucleus to the cytoplasm [5,6]. Our data suggest that these underlying mechanistic differences influence the steady-state levels of proteins like Por1, which could interfere with mitochondrial function and respiratory growth.

The results in yeast led us to address whether mitochondrial function is affected in a human cell line model of SDS. To this end, we used the human erythroleukemia cell line TF-1, infected with lentiviral vectors expressing shRNAs to SBDS mRNA. These cells express very low levels of SBDS and exhibit a modest increase in VDAC1, the human ortholog of Por1. We assessed mitochondrial function in these cells by monitoring both mitochondrial

membrane potential and oxygen consumption. The membrane potential in cells depleted of SBDS was reduced by approximately 15% relative to scrambled controls. Similarly, oxygen consumption was reduced in TF-1 cells depleted of SBDS. These data indicate that mitochondrial function is impaired in TF-1 cells expressing reduced levels of SBDS protein.

The compromised mitochondrial function in cells depleted of SBDS is intriguing in view of recent results suggesting a role for reactive oxygen species in SDS pathophysiology [9]. Since mitochondria are a major source of reactive oxygen species in cells and disruptions of mitochondrial function can enhance ROS production [27], we sought to determine whether ROS generation was increased in TF-1 cells depleted of SBDS. Our data showing an increase in ROS generation are consistent with a role for mitochondrial dysfunction as potential source of ROS in cellular models of SDS.

Pearson's syndrome is caused by mutations in mitochondrial DNA and is characterized by bone marrow failure (typically, anemia or pancytopenia) and defective exocrine pancreas function, reminiscent of the cardinal pathologies seen in SDS. ROS production has also been linked with hematopoietic stem cell aging, as well as bone marrow failure disorders such as SDS. However, our current work is the first to describe mitochondrial dysfunction in cells depleted of SBDS. Together, our findings uncover a new physiologic function for SBDS, to add to its reported roles in ribosome synthesis, chemotaxis, and mitotic spindle assembly.

Acknowledgment

This work was supported by a grant from the Shwachman Diamond Project.

Appendix A. Supplementary data

Supplementary data associated with this article can be found, in the online version, at http://dx.doi.org/10.1016/j.bbrc.2013.06.028.

References

[1] L. Burroughs, A. Woolfrey, A. Shimamura, Shwachman-Diamond syndrome: a review of the clinical presentation, molecular pathogenesis, diagnosis, and treatment, Hematol. Oncol. Clin. North Am. 23 (2009) 233–248.
[2] G.R. Boocock, J.A. Morrison, M. Popovic, N. Richards, L. Ellis, P.R. Durie, J.M. Rommens, Mutations in SBDS are associated with Shwachman-Diamond syndrome, Nat. Genet. 33 (2003) 97–101.
[3] T.F. Menne, B. Goyenechea, N. Sanchez-Puig, C.C. Wong, L.M. Tonkin, P.J. Ancliff, R.L. Brost, M. Costanzo, C. Boone, A.J. Warren, The Shwachman-Bodian-Diamond syndrome protein mediates translational activation of ribosomes in yeast, Nat. Genet. 39 (2007) 486–495.
[4] J.B. Moore, J.E. Farrar, R.J. Arceci, J.M. Liu, S.R. Ellis, Distinct ribosome maturation defects in yeast models of Diamond-Blackfan anemia and Shwachman-Diamond syndrome, Haematologica 95 (2010) 57–64.
[5] A.J. Finch, C. Hilcenko, N. Basse, L.F. Drynan, B. Goyenechea, T.F. Menne, A. Gonzalez Fernandez, P. Simpson, C.S. D'Santos, M.J. Arends, J. Donadieu, C. Bellanne-Chantelot, M. Costanzo, C. Boone, A.N. McKenzie, S.M. Freund, A.J. Warren, Uncoupling of GTP hydrolysis from eIF6 release on the ribosome causes Shwachman-Diamond syndrome, Genes Dev. 25 (2011) 917–929.
[6] C.C. Wong, D. Traynor, N. Basse, R.R. Kay, A.J. Warren, Defective ribosome assembly in Shwachman-Diamond syndrome, Blood 118 (2011) 4305–4312.
[7] K.M. Austin, M.L. Gupta, S.A. Coats, A. Tulpule, G. Mostoslavsky, A.B. Balazs, R.C. Mulligan, G. Daley, D. Pellman, A. Shimamura, Mitotic spindle destabilization and genomic instability in Shwachman-Diamond syndrome, J. Clin. Invest. 118 (2008) 1511–1518.
[8] D. Wessels, T. Srikantha, S. Yi, S. Kuhl, L. Aravind, D.R. Soll, The Shwachman-Bodian-Diamond syndrome gene encodes an RNA-binding protein that localizes to the pseudopod of Dictyostelium amoebae during chemotaxis, J. Cell Sci. 119 (2006) 370–379.
[9] C. Ambekar, B. Das, H. Yeger, Y. Dror, SBDS-deficiency results in deregulation of reactive oxygen species leading to increased cell death and decreased cell growth, Pediatr. Blood Cancer 55 (2010) 1138–1144.
[10] V. Shoshan-Barmatz, V. De Pinto, M. Zweckstetter, Z. Raviv, N. Keinan, N. Arbel, VDAC, a multi-functional mitochondrial protein regulating cell life and death, Mol. Aspects Med. 31 (2010) 227–285.
[11] B. Futcher, G.I. Latter, P. Monardo, C.S. McLaughlin, J.I. Garrels, A sampling of the yeast proteome, Mol. Cell. Biol. 19 (1999) 7357–7368.
[12] J.L. Campian, X. Gao, M. Qian, J.W. Eaton, Cytochrome C oxidase activity and oxygen tolerance, J. Biol. Chem. 282 (2007) 12430–12438.
[13] X. Gao, M. Qian, J.L. Campian, J. Marshall, Z. Zhou, A.M. Roberts, Y.J. Kang, S.D. Prabhu, X.F. Sun, J.W. Eaton, Mitochondrial dysfunction may explain the cardiomyopathy of chronic iron overload, Free Radic. Biol. Med. 49 (2010) 401–407.
[14] E. Blachly-Dyson, J. Song, W.J. Wolfgang, M. Colombini, M. Forte, Multicopy suppressors of phenotypes resulting from the absence of yeast VDAC encode a VDAC-like protein, Mol. Cell. Biol. 17 (1997) 5727–5738.
[15] F. Sherman, Getting started with yeast, Methods Enzymol. 194 (1991) 3–21.
[16] G. Sezgin, A.L. Henson, A. Nihrane, S. Singh, M. Wattenberg, P. Alard, S.R. Ellis, J.M. Liu, Impaired growth, hematopoietic colony formation, and ribosome maturation in human cells depleted of Shwachman-Diamond syndrome protein SBDS, Pediatr. Blood Cancer 60 (2013) 281–286.
[17] N. Koitabashi, D.A. Kass, Reverse remodeling in heart failure-mechanisms and therapeutic opportunities, Nat. Rev. Cardiol. 9 (2011) 147–157.
[18] S. Hoppins, S.R. Collins, A. Cassidy-Stone, E. Hummel, R.M. Devay, L.L. Lackner, B. Westermann, M. Schuldiner, J.S. Weissman, J. Nunnari, A mitochondrial-focused genetic interaction map reveals a scaffold-like complex required for inner membrane organization in mitochondria, J. Cell Biol. 195 (2011) 323–340.
[19] S.P. Mathupala, P.L. Pedersen, Voltage dependent anion channel-1 (VDAC-1) as an anti-cancer target, Cancer Biol. Ther. 9 (2010) 1053–1056.
[20] I. Koren, Z. Raviv, V. Shoshan-Barmatz, Downregulation of voltage-dependent anion channel-1 expression by RNA interference prevents cancer cell growth in vivo, Cancer Biol. Ther. 9 (2010) 1046–1052.
[21] H. Galganska, A. Karachitos, M. Wojtkowska, O. Stobienia, M. Budzinska, H. Kmita, Communication between mitochondria and nucleus: putative role for VDAC in reduction/oxidation mechanism, Biochim. Biophys. Acta 1797 (2010) 1276–1280.
[22] H. Galganska, A. Karachitos, M. Baranek, M. Budzinska, J. Jordan, H. Kmita, Viability of *Saccharomyces cerevisiae* cells following exposure to H_2O_2 and protective effect of minocycline depend on the presence of VDAC, Eur. J. Pharmacol. 643 (2010) 42–47.
[23] A.D. Chacko, F. Liberante, I. Paul, D.B. Longley, D.A. Fennell, Voltage dependent anion channel-1 regulates death receptor mediated apoptosis by enabling cleavage of caspase-8, BMC Cancer 10 (2010) 380.
[24] B.M. McDonald, M.M. Wydro, R.N. Lightowlers, J.H. Lakey, Probing the orientation of yeast VDAC1 in vivo, FEBS Lett. 583 (2009) 739–742.
[25] H. Galganska, M. Budzinska, M. Wojtkowska, H. Kmita, Redox regulation of protein expression in *Saccharomyces cerevisiae* mitochondria: possible role of VDAC, Arch. Biochem. Biophys. 479 (2008) 39–45.
[26] S.L. Mi, C.C. An, Y. Wang, J.Y. Chen, N.Y. Che, Y. Gao, Z.L. Chen, Trichomislin, a novel ribosome-inactivating protein, induces apoptosis that involves mitochondria and caspase-3, Arch. Biochem. Biophys. 434 (2005) 258–265.
[27] G.D. Zeevalk, L.P. Bernard, C. Song, M. Gluck, J. Ehrhart, Mitochondrial inhibition and oxidative stress: reciprocating players in neurodegeneration, Antioxid. Redox Signal. 7 (2005) 1117–1139.